Experimental assessment of RC exterior beam-column joints without transverse reinforcement

M. T. De Risi, P. Ricci & G. M. Verderame
Department of Structures for Engineering and Architecture, University of Naples Federico II, Italy

Abstract

In the assessment of the performance of typical existing buildings, seismic collapse safety might be significantly affected by the non-linear behaviour of the joints that are involved in the failure mechanisms, especially if they are characterized by poor structural detailing, such as the lack of an adequate transverse reinforcement in the joint panel.

Many retrofit strategies for existing joints are available, but commonly accepted tools to assess existing joint capacity – which is the starting point for retrofit – are not available. Few reliable approaches for modelling all sources of nonlinearity are proposed in literature for poorly designed beam-column joints because of relatively poor information from experimental tests.

The current study aims to improve the understanding of exterior joint seismic performance without transverse reinforcement in existing RC buildings through experimental tests.

Two full-scale exterior unreinforced beam-column joint sub-assemblages are tested under cyclic loading. Two different kinds of joint failure are expected, with or without the yielding of the adjacent beam, basically depending on the beam longitudinal reinforcement ratio. Strain gauges located on beam bars and LVDTs on the joint panel allow the complete definition of the deformability contributions.

Design criteria, adopted setup and main experimental results are described.
Keywords: exterior RC joint, non-conforming, experimental, shear strength, shear strain.

WIT Transactions on The Built Environment, Vol 152, © 2015 WIT Press
www.witpress.com, ISSN 1743-3509 (on-line)
doi:10.2495/ERES150201

1 Introduction

Reinforced Concrete (RC) buildings designed for gravity loads only or according to obsolete seismic codes are widespread in Italian and Mediterranean building stock. For these buildings, beam-column joints represent a critical issue; the lack of capacity design principles leads to a low shear strength of the joint, potentially leading to a shear failure that limits the deformation capacity of adjoining beams and/or columns [1, 2].

Past earthquakes showed that shear failure of beam-column joints can lead to building collapse [3] which often can be attributed to inadequate joint confinement. In recent earthquakes all around the word (Izmit earthquake [4], Tehuacan earthquake [5], Chi-Chi earthquake [6], the inadequacy of building joints designed according to earlier rather than more current standards was one of the main causes of severe damages or collapses. In particular, the observations of damage after the 2009 L'Aquila earthquake [7] indicated that some RC buildings designed in Italy before the mid-1990s may have serious structural deficiencies especially in joint regions, mainly due to a lack of capacity design approach and/or poor detailing of reinforcement.

Several researchers have focused their attention on different parameters influencing the response of unreinforced beam-column joints, such as column axial load, concrete strength, joint aspect ratio, beam longitudinal reinforcement ratio. However, further research is steel needed. As a matter of fact, for instance, in most of the tests the focus was given to the ultimate shear strength of the joint; only few authors have measured joint shear strain – e.g. [8, 9] for plain exterior joints or [10] and [1] for corner joints. However, a complete characterization of the nonlinear local response of the joint panel and fixed-end-rotation contribution is necessary to understand clearly beam-column joint behaviour also within the context of a RC frame.

This study aims to improve the understanding of exterior joints seismic performance without transverse reinforcement in existing RC buildings through two experimental tests, different for failure typology, analyzing also local shear stress-strain response of the joint panel. A comparison with main literature capacity models for joint shear strength is reported, too.

2 Experimental program and setup

Two full-scale exterior unreinforced beam-column joint sub-assemblages have been tested under cyclic loading. The two specimens are different for beam longitudinal reinforcement ratio and they are both reinforced with deformed bars. Specimens were designed to obtain two different kinds of joint failure, with or without the yielding of the adjacent beam.

Columns were designed according to capacity design principles in order to obtain a weak beam-strong column hierarchy. Beam longitudinal reinforcement was designed to observe joint shear failure prior to (Test #1) or following (Test #2) beam yielding. Stirrup spacing in beam and column was designed to

avoid shear failure, while no transverse reinforcement is located in the joint panel zone.

The two tests are identical for geometry: the beam is 50cm wide and 30cm deep and the column section is 30×30cm^2.

As shown in Figure 1, in Test #1 the beam is symmetrically reinforced with 4ϕ20 bars for both reinforcement layers (corresponding to a compression and tension reinforcement ratio equal to ρ'=ρ=0.84%); also column is symmetrically reinforced with 4ϕ20 bars for top and bottom sides, corresponding to a total reinforcement ratio (ρ'+ρ) equal to 2.79%. In Test #2, the beam is symmetrically reinforced with 4ϕ12 bars for both the positive and negative (corresponding to a compression and tension reinforcement ratio equal to ρ'=ρ=0.30%); also column is symmetrically reinforced with 4ϕ12 bars for top and bottom sides, corresponding to a total reinforcement ratio (ρ'+ρ) equal to 1.01%.

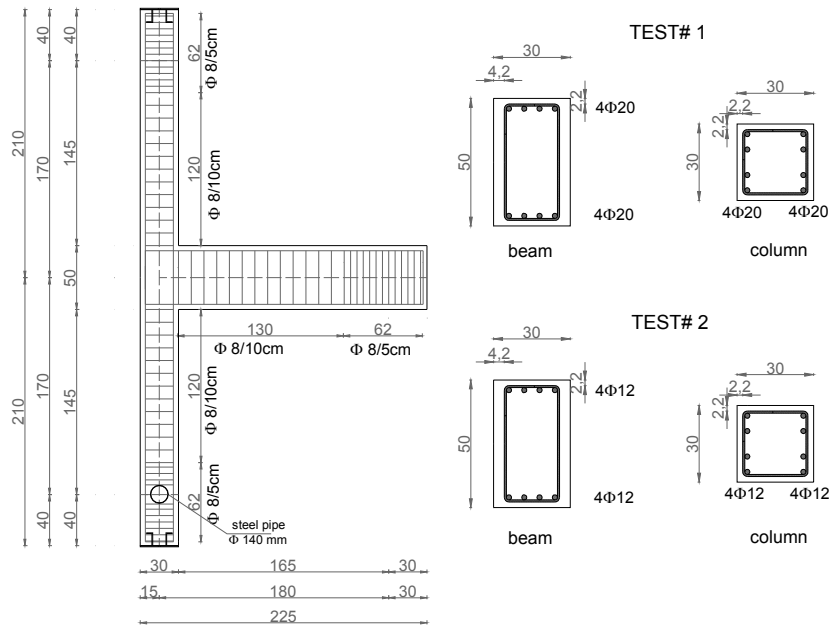

Figure 1: Geometry and reinforcement details.

In both cases, top and bottom beam longitudinal bars are hooked bent at 90° into the joint core for a length of 20 cm. The transverse reinforcement consists of an 8 mm diameter closed stirrup with 90° bent and 10cm extension on both ends. The stirrups are spaced at 10cm along the beam and the column except within 62 cm of beam and column end, where the spacing is reduced to 5cm to give adequate strength at the location where forces are applied during the test. The longitudinal reinforcement in the column extends continuously up through the joint from the bottom to the top of the column.

Column length was designed to be representative of typical interstorey height (3.40m) and beam length (1.80m) is intended to be representative of a portion up to a zero point of bending moment diagram in frames designed for gravity loads.

2.1 Materials

Concrete compressive strength for all specimens was evaluated on four 15×15×15cm cubic samples of the casted concrete. Values of 28-day mean cylindrical strength is f_{cm}=28.80MPa.

Commercial typology of reinforcing steel adopted is B450C [11], i.e., class C reinforcement with f_{yk}=450MPa according to Annex C provisions of Eurocode 2 [12]. Tensile tests were carried out on three samples for each bar diameter. Table 1 reports mean values of their mechanical properties, namely yield strength (f_y), ultimate strength (f_t) and hardening ratio (f_t/f_y).

Table 1: Properties of steel.

Diameter [mm]	Yield strength (f_y) [MPa]	Ultimate strength (f_t) [MPa]	Hardening ratio (f_t/f_y) [-]
20	486.5	595.5	1.22
12	459.1	559.7	1.22
8	492.0	606.8	1.23

2.2 Test setup

A schematic of the loading apparatus is shown in Figure 2(a). The column was mounted horizontally with pinned supports at both ends and the specimen was constrained to the strong floor by means of two rigid steel frames. Steel spherical hinges were placed between the beam end and floor to limit friction and to allow tip beam free movement. The axial load was applied using a small hydraulic jack in load control and transferred to the column through a system constituted by four pre-stressed rods connected to strong steel plates located on the top and bottom of the column. In particular, a constant value of axial load equal to 260kN (corresponding to an axial load ratio equal to 0.10) was adopted.

A hydraulic actuator applied the lateral load in displacement control at the end of the beam by means of a loading collar. A load cell situated between the hydraulic actuator and the loading collar measured the quasi-static cyclic load applied to the beam. The actuator was pinned at the end to allow rotation during the test.

Twelve Linear Potentiometer sensors (LPs) adopted to measure joint shear strain and fixed-end-rotations were located in the joint panel along longitudinal reinforcement layers of beam and column and along the diagonals of the joint panels, as shown in Figure 2(b). A wire potentiometer was placed at the end of the beam to measure beam deflection.

Strains in beam longitudinal reinforcement were measured, too, by means of six strain gauges (sgs) located as shown in Figure 2(c) (three on a bar in the top layer and three on a bar in the bottom layer). Two additional Linear Variable Displacement Transducers (LVDTs) located along beam deep were used in Test #2 in order to have a more reliable measure of beam fixed-end-rotation contribution.

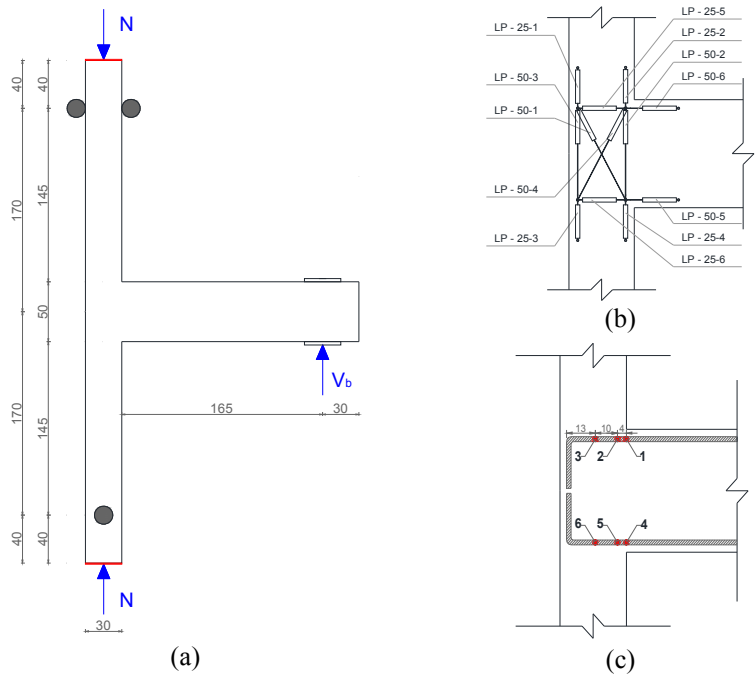

Figure 2: Test setup (a), joint panel instrumentation (b) and strain gauges location (c).

2.3 Load pattern

Before beginning each test, the axial load was slowly applied to the column until the appropriate level was achieved. Then, the lateral load was applied cyclically, in a quasi-static way, at the end of the beam. The loading procedure consisted of displacement-controlled steps beginning at a 0.25% drift followed by steps of 0.50%, 0.75%, 1.00%, 1.50%, 2.00%, 3.00%, 4.00% and 6.00% drift. Each drift step consisted of 3 cycles of push and pull.

3 Experimental results

Lateral load-displacement response of tested specimens is analyzed, and the evolution of observed damage with increasing imposed displacement is described.

Test #1
Test #1 exhibited an initial uncracked stiffness, calculated as the secant to the experimental backbone in its first point, equal to 15.0kN/mm. Such a stiffness slightly decreased up to 12.7kN/mm in the first millimetre of displacement applied to the beam end, and showed a more significant reduction when the

applied drift ranges between 0.50% and 0.75%, when first joint panel cracking occurred. Experimental response was quite symmetric during the push-pull cycles. Peak load was reached for a drift equal to 1.40% for positive loading direction and -1.38% for negative loading direction. Peak values of beam lateral load were 74.0kN and -72.4kN, respectively for positive and negative loading direction. Since beam yielding is expected to occur for a beam lateral load value of 155.6kN, such a test can be classified as J-failure, namely joint shear failure occurs before yielding of beam. Such a classification will be confirmed by the measures of bar strains provided by the adopted strain gauges.

When the test was interrupted (first cycle at 6.00% drift) the strength reduction (evaluated on the backbone of the response) was equal to 47% and 53%, respectively in positive and negative directions. Beam lateral load versus drift response related to Test #1 is reported in Figure 3(a).

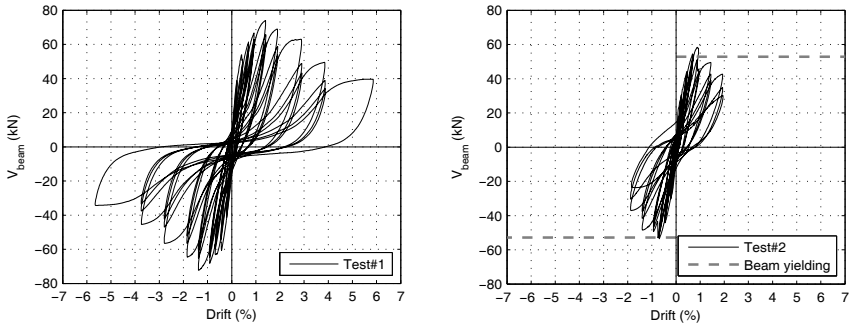

Figure 3: Beam lateral load-drift response: Test #1 (a), Test#2 (b).

Test #2

Test #2 exhibited an initial uncracked stiffness, calculated as the secant to the experimental backbone in its first point, equal to 15.1kN/mm. Such a stiffness decreased up to 14.5kN/mm in the first millimetre of displacement applied to the beam end, and showed a more significant reduction when the applied drift ranges between 0.25% and 0.50%, when first cracks along beam-joint interface started to occur. Experimental response is quite symmetric during the push-pull cycles. Peak load was reached for a drift equal to 0.88% for positive loading direction and -0.69% for negative loading direction. Peak values of beam lateral load were 58.33kN and -53.27kN, respectively for positive and negative loading direction. Since beam yielding was expected to occur for a beam lateral load value of 52.9kN, such a test can be classified as BJ-failure, namely joint shear failure occurs after yielding of beam. Such a classification was confirmed by the measures of bar strains provided by the adopted strain gauges.

Test #2 was interrupted when the three cycles at 2.00% drift were fully completed because the hydraulic jack could not more sustain in safe the column axial load. When the test was interrupted the strength reduction (evaluated on the backbone of the response) was equal to 27% and 31%, respectively in positive

and directions. Beam lateral load versus drift response related to Test #2 is reported in Figure 3(b). Peak values of beam lateral load for positive ($V^{+}_{b,max}$) and negative ($V^{-}_{b,max}$) loading directions and corresponding drifts are summarized in Table 2, together with beam load value corresponding to beam yielding.

Table 2: "Peak points" and yielding beam load.

	$V^{+}_{b,max}$ [kN]	Drift at peak $^{+}$ [%]	$V^{-}_{b,max}$ [kN]	Drift at peak $^{-}$ [%]	$V_{b,yield}$ [kN]
Test #1	74.0	1.40	-72.4	-1.38	155.6
Test #2	58.3	0.88	-53.3	-0.69	52.9

3.1 Observed damage

Test #1
First cracks in the joint panel appeared at a drift ratio equal to 0.50%. Diagonal cracks in the joint panel occurred and spread along column longitudinal bars between 0.50% and 0.75% drift. At 2.00%, cracks at beam-joint interface appeared and increased progressively their width, mainly due to fixed-end-rotation of the beam. At 3.00% drift, existing cracks in the joint panel increased their width and concrete cover spalling started to occur from a corner. Concrete cover spalling was complete when a drift value of 6.00% was reached

Test #2
First cracks appeared at beam-joint interface at 0.50% drift. At 1.00%, diagonal cracks in the joint panel occurred and spread along column longitudinal bars. At 1.50%, cracks at beam-joint interface widened, mainly due to fixed-end-rotation of the beam, and new diagonal cracks appeared in the joint core. At 2.00%, existing cracks significantly widened and buckling of longitudinal bars of column and sudden complete cover spalling occurred at the third step of the sixth cycle. The hydraulic jack was no longer able to sustain column axial load safely.

Tables 3 and 4 summarize the evolution of the observed damage described above; Figure 4 shows the final damage state of the specimens.

3.2 Joint panel response

Linear potentiometers located on the joint panel are employed to calculate joint shear strain, as suggested by previous experimental studies (e.g. [13] and [10]). Joint shear strain can be expressed as shown in eqn (1)

$$\gamma_{s,i} = \frac{\varepsilon_\theta - \varepsilon_x \cos^2\theta - \varepsilon_y \sin^2\theta}{\sin\theta\cos\theta} \tag{1}$$

where $\gamma_{s,i}$ is the joint shear strain obtained using a certain set of strain measures, ε_x and ε_z are strains in the horizontal and vertical directions, respectively, and ε_θ is the strain in the diagonal direction with an angle of θ measured from the

Table 3: Description of the evolution of joint damage during Test #2.

Cycle	Drift [%]	Joint damage
1	0.25	No damage
2	0.50	First light cracks at panel corners
3	0.75	Diagonal cracks in the joint panel spreading along column longitudinal bars
4	1.00	New diagonal cracks and spreading of existing cracks
5	1.50	New diagonal cracks
6	2.00	New diagonal cracks
7	3.00	Spreading of existing cracks and beginning of concrete cover spalling starting from panel corners
8	4.00	New diagonal cracks, significant cracks lengthen, concrete cover spalling
9	6.00	Complete concrete cover spalling

Table 4: Description of the evolution of damage during Test #1.

Cycle	Drift [%]	Joint damage
1	0.25	No damage
2	0.50	No damage
3	0.75	No damage
4	1.00	Light diagonal cracks in the joint panel
5	1.50	New diagonal cracks in the joint panel and light cracks along column longitudinal bars
6-1	2.00	New diagonal cracks in the joint panel
6-2	2.00	Significant lengthening of existing cracks
6-3	2.00	Concrete cover spalling along external panel side

(a)

(b)

Figure 4: Final damage state joint panel and beam-joint interface: Test#1 (a) and Test#2 (b).

horizontal axis. Four estimates of the joint shear strain were obtained by four triangles of LPs located in the joint panel, see Figure 2(b), by using eqn (1). Joint shear strain (γ_{joint}) is finally calculated as the mean of these four estimates.

Joint shear stress is calculated on the basis of equilibrium equations, in conjunction with strain gauges measures. In particular, joint shear V_{jh} is calculated as shown in eqn (2)

$$V_{jh} = T - V_c \tag{2}$$

where T is the tensile force acting in beam longitudinal bars and V_c represents column shear force. Tensile force T is obtained as shown in eqn (3)

$$T = \varepsilon_s E_s A_s \leq \varepsilon_{s,y} E_s A_s \tag{3}$$

where ε_s is the strain measure obtained from strain gauges located at beam-joint interface (sgs #1 and #4), A_s is the area of longitudinal tensile bars of beam and E_s represents the Young modulus of steel. Column shear force V_c is calculated from the equilibrium of the subassemblage represented by the specimen.

Joint shear stress (τ_{joint}) can be calculated as the ratio between joint shear force (V_{jh}) and joint horizontal area (A_{jh}). Herein after, τ_{joint} will represents joint shear stress divided by the square root of concrete strength f_c. In Figure 5, (τ_{joint}) versus joint strain (γ_{joint}) experimental responses are reported for Test #1 and #2, respectively. Data are represented until LPs measures are considered reliable, i.e. until cracks significantly involved the supported points of LPs.

In Test #1, the peak values of τ_{joint} are 0.63 and -0.62 $(MPa)^{0.5}$ for positive and negative direction, respectively. The corresponding γ_{joint} are equal to 0.53% and -1.18%.

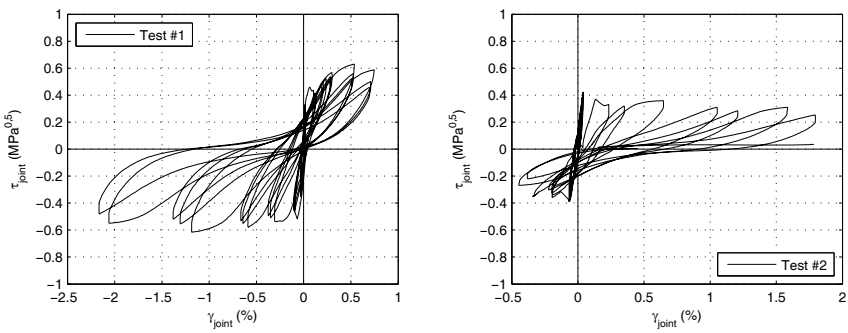

Figure 5: Joint shear stress–strain experimental response: Test #1 (a) and Test#2 (b).

In Test #2, the peak values of τ_{joint} are 0.42 and -0.39 $(MPa)^{0.5}$ for positive and negative direction, respectively. The corresponding γ_{joint} are equal to 0.04% and -0.07%. These peak points were reached at the end of the elastic phase of behaviour of the joint that has a high (pre-cracking) stiffness.

4 Joint shear strength: comparison with literature models

Local joint panel responses of Tests #1 and #2 are compared with strength models existing in literature. Figure 6(a) and (b) shows the envelope of the experimental shear stress-strain joint response related to Test#1 and Test#2, respectively. Experimental peak strength ($\tau_{joint,max}$) is compared with joint strength predicted by some of the more diffused formulations from codes and literature, namely:

- ASCE-SEI/41 [14], providing $\tau_{joint,max}$ depending on the joint typology and the transverse reinforcement ratio (equal to $0.5MPa^{0.5}$ for unreinforced exterior joints without transverse beams);
- Priestley [15], which suggests to limit the maximum value of principal tensile stress to $0.42 \cdot f_c^{0.5}$;
- Park and Mosalam [1], a mechanical approach accounting for joint shear strength degradation after beam yielding and directly providing a definition of the failure mode.

Test#1

In Figure 6(a), it can be observed that the code proposal adopted herein as a reference [14] underestimates the experimental strength. The model that better predicts experimental strength is model by Priestley [15]. Finally, model by Park and Mosalam [1] overestimates the maximum strength: the ratio between predicted and experimental shear strength is equal to 1.14.

Since Test#1 exhibited J-failure mode, joint stress corresponding to beam yielding is about two times the peak experimental value.

Test#2

Figure 6(b) shows the envelope of the experimental shear stress-strain joint response related to Test #2 and joint strength values predicted by the models mentioned above. In this case, the model by Park and Mosalam [1] shows the better agreement with experimental response: the ratio between predicted and experimental shear strength is equal to 0.97.

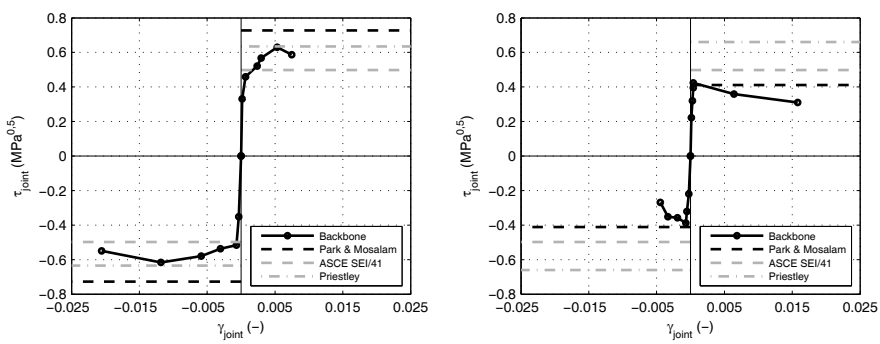

Figure 6: Joint shear stress-strain: envelope and comparison between experimental response and strength models from literature for Test #1 (a) and Test#2 (b).

Joint shear stress corresponding to beam yielding is lower than the peak experimental value, thus confirming the classification of Test #2 as a BJ-failure mode. Note that in this test yielding of beam longitudinal bars is observed very close to cracking of joint panel [16], at peak strength, after which a strength decrease is shown.

A summary of joint shear strength from different models for Test #1 and Test #2 is reported in Table 5.

Table 5: Experimental joint shear strength and models from literature.

Joint shear stress [$MPa^{0.5}$]						
	Exp. strength	ASCE/SEI 41 [14]	Priestley [15]	Park and Mosalam [1]	Predicted cracking [16]	Predicted yielding
Test#1	0.641	0.5	0.635	0.728	0.39	1.30
Test#2	0.423	0.5	0.660	0.412	0.39	0.38

5 Conclusions

Experimental results of two test on unreinforced exterior RC beam-column joints were shown. Tests were designed in order to show failure of joint panel prior to (Test #1) or following (Test #2) yielding of longitudinal bars. Experimental results show, in Test #1, that the attainment of maximum strength and the post-peak degrading behaviour are controlled by joint failure, without flexural yielding of the beam, as expected. In Test #2 complete failure is attained corresponding to buckling of longitudinal bars of column and sudden complete cover spalling, together with observed failure of anchorage of beam longitudinal bars.

The experimental tests described herein can provide a very useful contribution to the characterization of the experimental behaviour of unreinforced RC beam-column joints, in order to validate/propose capacity models for the assessment of existing non-ductile RC buildings.

References

[1] Park S and Mosalam KM, (2012) “Analytical model for predicting the shear strength of unreinforced exterior beam-column joints”, ACI Structural Journal 109, 149–159.

[2] Celik OC and Ellingwood BR (2008) “Modeling Beam-Column Joints in Fragility Assessment of Gravity Load Designed Reinforced Concrete Frames”, Journal of Earthquake Engineering. 12:357-381.

[3] Moehle, J.P. and Mahin, S.A. 1991. Observations on the behavior of reinforced concrete buildings during earthquakes. Earthquake-Resistant Concrete Structures Inelastic Response and Design SP-127, American Concrete Institute, ed. S.K. Ghosh, Detroit.

[4] Sezen, H., Elwood, K.J., Whittaker, A.S., Mosalam, K. M., Wallace, J.W., and Stanton, J.F. 2000. Structural engineering reconnaissance of the August 17, 1999 earthquake: Kocaeli (Izmit), Turkey, PEER-2000/09, Berkeley:

Pacific Earthquake Engineering Research Center, University of California, Dec.
[5] Earthquake Engineering Research Institute. 1999a. EERI Special Earthquake Report – September 1999. The Tehuacan, Mexico, Earthquake of June 15, 1999. http://www.eeri.org/
[6] Earthquake Engineering Research Institute. 1999b. EERI Special Earthquake Report – December 1999. The Chi-Chi, Taiwan Earthquake of September 21, 1999. http://www.eeri.org/
[7] Ricci P., De Luca F., Verderame G.M., 2011. 6th April 2009 L'Aquila earthquake, Italy: reinforced concrete building performance. Bulletin of Earthquake Engineering. Vol. 9, Issue 1, pp. 285-305.
[8] Clyde C, Pantelides CP, Reaveley LD (2000) "Performance-Based Evaluation of Exterior Reinforced Concrete Buildings Joints for Seismic Excitation", PEER Report, No. 2000/05, Pacific Earthquake Engineering Research Center, University of California, Berkeley, USA.
[9] Pantelides CP, Hansen J, Nadauld J, Reaveley LD (2002) "Assessment of Reinforced Concrete Building Exterior Joints with Substandard Details", PEER Report, No. 2002/18, Pacific Earthquake Engineering Research Center, University of California, Berkeley, USA.
[10] Hassan WM (2011) "Analytical and Experimental Assessment of Seismic Vulnerability of Beam-Column Joints without Transverse Reinforcement in Concrete Buildings", PhD Dissertation, University of California, Berkeley, California, USA.
[11] Decreto Ministeriale del 14/1/2008. Approvazione delle nuove norme tecniche per le costruzioni. G.U. n. 29 del 4/2/2008, 2008. (in Italian)
[12] CEN, 2004. European standard EN1992-1-1. Eurocode 2: Design of concrete structures - Part 1-1: General rules and rules for buildings. Comité Européen de Normalisation, Brussels.
[13] Engindeniz, M. (2008) "Repair and Strengthening of Pre-1970 Reinforced Concrete Corner Beam-Column Joints Using CFRP Composites", PhD Thesis, Civil and Environmental Engineering Department, Georgia Institute of Technology, August 2008.
[14] ASCE/SEI 41, Seismic rehabilitation of existing buildings. American Society of Civil Engineers, Reston, VA, USA, 2007.
[15] Priestley, M.J.N. (1997) "Displacement-based seismic assessment of reinforced concrete buildings". Journal of earthquake Engineering 1: 157-192.
[16] Uzumeri SM (1977) "Strength and ductility of cast-in-place beam-column joints". From the American Concrete Institute Annual Convention, Symposium on Reinforced Concrete Structures in Seismic Zones, San Francisco, 1974. No. SP-53.